Aerodynamic Optimisation of the AW101 Heavy Helicopter Engine Installation by means of a Multi-objective Approach

A. Garavello[1], M. Russo[2], Claudio Comis da Ronco[3], R.Ponza[4], E. Benini[5], A. Ramage[6]

[1] Research Engineer, HIT09 S.r.l, a.garavello@hit09.com

[2] Research Engineer, HIT09 S.r.l, m.russo@hit09.com

[3] Research Engineer, University of Padova, claudio.comis@unipd.it

[4] Senior Research Engineer, HIT09 S.r.l, r.ponza@hit09.com

[5] Associate Professor, University of Padova, HIT09 S.r.l, ernesto.benini@unipd.it

[6] Principal Engineer - Fuselage Aerodynamics, AgustaWestland, andrew.ramage@agustawestland.com

Aerodynamic design and optimisation of engine installations is an important part of the helicopter design process. Total pressure loss reduction, together with the optimisation of the flow pattern at the engine intake aerodynamic interface plane, increases the global engine efficiency and results in lower fuel consumption. At the same time, a reduction of the engine exhaust back pressure corresponds to an increase of the installed engine power output that is particularly valuable in the hover flight condition. In such context the application of advanced optimisation algorithms coupled with CFD solvers for an accurate flow solution represents a very powerful tool for parametric design and optimisation of engine installation components. Because of the above mentioned reasons, the consortium constituted by the University of Padova (UNIPD) and the spin-off company HIT09 developed an automatic optimisation loop based on the genetic algorithm GDEA, which is applicable to engine installation design as well as to general aircraft and rotorcraft component optimisation problems. The application of the GDEA-based optimisation loop to the multi-objective, multi-point design and optimisation of the AgustaWestland AW101 helicopter air intake system is described in this paper; the results presented demonstrate the effectiveness of parametric design and optimisation methods within helicopter engine installation design.

1. INTRODUCTION

Within the Clean Sky framework, a joint technical initiative funded by the European Commission and industry, a specific activity is dedicated to the study of the engine installation design of heavy helicopters. A consortium consisting of the University of Padova and the spin-off companies HIT09 and MDA submitted the HEAVYcOPTer project proposal in response to a specific Call on the subject [1]. The Call, specified by AgustaWestland, asked for a partner able to contribute and to support the Clean Sky Industry Partners in accomplishing the aerodynamic optimisation of the engine intake and exhaust of a heavy helicopter. HEAVYcOPTer was selected to meet the Call by a committee of experts appointed by the Clean Sky Joint Undertaking. HEAVYcOPTer started on 1st April 2011, with a duration of two years and this paper describes the current progress within the HEAVYcOPTer project. HEAVYcOPTer is devoted to the efficient design and the shape optimisation of the AgustaWestland AW101 engine intake and exhaust system, carried out by means of advanced multi-objective optimisation algorithms coupled with CFD Navier-Stokes solvers [1].

Efficient aerodynamic design of air intakes is a challenging objective for airframe manufacturers: inlet

The research leading to these results has received funding from the European Union's Seventh Framework programme (FP7 2007-2013) for the Clean Sky Joint Technology Initiative.

flow typically develops in adverse pressure gradient conditions, which leads to boundary layer instability and possible flow separation. Therefore inlet cross sectional area distribution along the central line should be optimised in order to minimise boundary layer "loading" and avoid separation [2]. In addition, for helicopter intake applications, an S-shaped duct is usually required to channel the air to the engine face; this is due to the presence of the engine shaft and the requirement for a short and compact duct layout. From the fluid-dynamic point of view, a curved duct induces a secondary flow pattern, which essentially sets up "pockets" of swirling flow at the duct exit [3] and causes engine performance degradation [4], [5]. In severe situations, these pockets of swirling flow can produce rotating stall instability of the compressor rotor [6]. Therefore, the internal shape of the curved duct should embody proper strategies in order to minimise total pressure loss and flow distortion at the engine face [7], [8]. Finally, stability of boundary layer in turboprop and helicopter inlets may also be remarkably affected by the aircraft operating conditions and flight speed [9], [10], [11]. In such a context CFD is a powerful tool which can be used to accurately evaluate the complex flow behaviour within inlet ducts: [12] and [13] are remarkable examples of CFD application to intake aerodynamics. When coupled with geometry parameterisation techniques, CFD provides an effective automatic design methodology for inlet ducts. For example, in [14] Zhang at all describe an automatic design method for 3D subsonic ducts using NURBS.

Within the HEAVYcOPTer framework, the base-line intake CFD model has been built up and validated by means of comparison against available wind tunnel experimental data, starting from the existing AW101 engine installation geometry provided by AgustaWestland Ltd. via CATIA® CAD models. CFD analysis has been carried out for nominal hover and forward flight cruise conditions; obtained results have been analysed in terms of total pressure losses, flow distortion, flow separation and all those aspects that affect the efficiency of the helicopter intake system. This accurate preliminary analysis allowed a proper understanding of the aerodynamic behaviour of the actual design and the identification of the most appropriate parametric changes to be applied to the geometry during the optimisation phase.

The baseline CFD solution and its associated parametric geometrical model are then the main inputs for the optimisation procedure selected, which involves the application of the innovative code GDEA (Genetic Diversity Evolutionary Algorithm) [15]. GDEA has been developed by the University of Padova and is a genetic algorithm able to perform multi-objective optimisation analysis with the general approach of the Pareto frontier search; it has been compared to other state of the art genetic algorithms with excellent results and, interfaced with flow solvers, it has been successfully used in several fluid-dynamics applications; in particular, within the Clean Sky GRC2 research program [16], a GDEA based optimisation loop has been successfully applied to several fuselage and engine installation components of the European tilt rotor ERICA [17]: the interested reader can find an extensive description of the main achievements of the Clean Sky GRC2 projects CODETilt [18] and TILTOp [19] in the conference papers [20], [21] and [22].

The results obtained by the application of the above mentioned optimisation chain on the AW101 engine installation are presented in this paper, with focus on the optimisation of the air intake number one, together with the description of future work, including engine intake number two and exhaust optimisation, which will be addressed within the remainder of the HEAVYcOPTer project.

2. DESCRIPTION OF THE OPTIMISATION METHOD

The aerodynamic optimisation procedure which has been implemented and is used for the project HEAVYcOPTer is structured in three phases as follows:

1) Baseline model preparation and simulation phase;
2) Automatic optimisation phase;
3) Post-processing and optimised CAD model reconstruction phase.

1.1 *Baseline model simulation*

Typically the starting point is represented by the CAD model of the baseline configuration. Starting from the geometrical model, the procedure moves into the "baseline simulation block" (see Figure 1), where the baseline configuration of the component under consideration must be analysed, in terms of aerodynamic performance in the most relevant operating conditions, via CFD computation using the selected flow solver. The assessment of the baseline solution allows the designer to properly understand the flow field characteristics of the geometry under analysis and gives fundamental indications for the optimisation objectives and constraints identification to inform the generation of the geometrical parametric model.

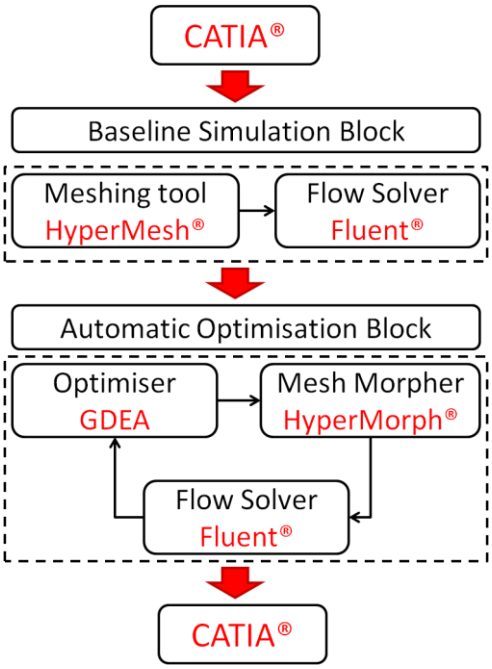

Figure 1: Optimisation method flow-chart.

1.2 *Automatic optimisation execution*

When the preliminary operations have been completed, the optimisation can be carried out by means of the automatic optimisation loop in Figure 1: it is constituted by the following components:

1) GDEA: an advanced multi-objective optimisation algorithm developed by the University of Padova [15]. It is the selected optimisation engine;
2) Altair HyperMorph® [23]: it makes possible to convert the design parameters coming out from GDEA into morphed CFD cases, suitable for the objective function evaluation;
3) Ansys Fluent® [24]: the selected flow solver; it takes as the input the morphed CFD cases coming from HyperMorph® and gives back to GDEA the correspondent values of the chosen objective functions.

During the optimisation process, GDEA lets a population of individuals "evolve" (each one corresponding to a different set of design variables and so to a different geometrical configuration) until the convergence to the *Pareto optimal frontier* has been reached. The Pareto frontier is the set of non-inferior solutions, which represents the solution of a multi-objective optimisation problem; a non-inferior solution, also called Pareto optimal or non-dominated solution, is one in which an improvement in one objective requires the degradation of another [25].

1.3 *Post-processing*

The Pareto frontier output from the automatic optimisation loop represents a multiple set of solutions equally optimal according to the Pareto concept ([15]) but of course different form the aerodynamic and engineering point of view. In fact each solution over the Pareto frontier may present advantages and drawbacks with respect the other solutions. In order to choose the most appropriate solution from among the optimal set post-processing work is necessary. Thanks to the intrinsic multi-objective approach adopted, the designer is allowed to select, among the Pareto optimal set, the solution which is most suitable for his needs: for example, choosing to privilege the improvement of one objective with respect to the other or even including other considerations such as non-aerodynamic requirements. The strength of the selected approach is that the designer can choose the proper trade-off between the objectives when the optimisation work has been completed and is not forced to introduce arbitrariness in the problem set up, as commonly happens using traditional optimisation approaches.

3. AW101 ENGINE INSTALLATION DESCRIPTION

The AW101 engine intake system comprises three side facing intake ducts feeding the three helicopter engines; from now on, we will refer to air intakes as "intake#1" and "intake#3" for the two symmetrical intakes on the fuselage sides, and "intake#2 for the intake placed at the top of the fuselage roof (Figure 2).

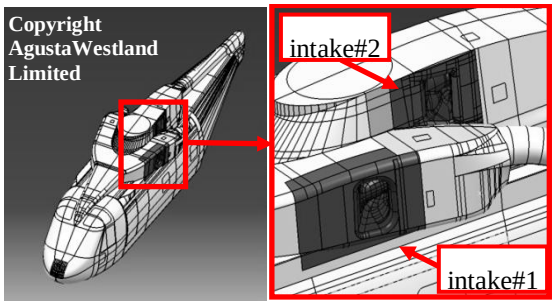

Figure 2: View of the AW101 CAD model geometry and zoomed view on intakes #1 and #2.

The objective of the project HEAVYcOPTer is to optimise the complete AW101 engine installation, however this paper only discusses the optimisation activities and results for intake#1.

Intake#1 is an S-shaped duct connecting the helicopter exterior flow field to the engine inlet, commonly referred as *Aerodynamic Interface Plane* (AIP). CAD layout of

engine bay#1 internal components was provided by AgustaWestland Ltd in order to allow the definition of geometrical modifications of the duct surfaces so as to be compliant with the installation architectural constraints (Figure 3).

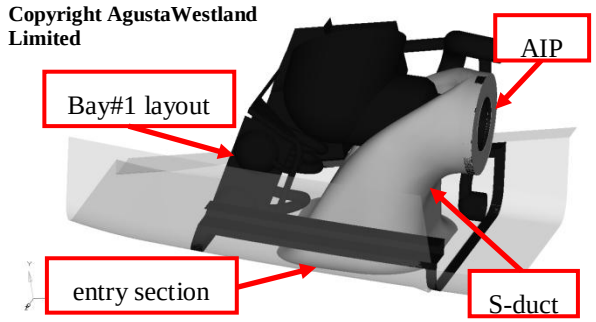

Figure 3: Internal view of intake#1 S-duct and bay#1 internal components layout.

4. AW101 INTAKE#1 CFD MODEL AND VALIDATION

The aerodynamic objective function for the optimisation problem is evaluated by means of Ansys Fluent®. In this work unstructured triangular surface meshes and tetra volume meshes with prismatic layer wall elements were used. An appropriate set of boundary conditions was chosen in order to represent the aircraft forward flight cruise and hover operating conditions; a mass flow outlet boundary condition was set at the outlet section of a "dummy duct" connected to the AIP in order to properly represent the engine effect over the intake flow field. The aircraft fuselage has been modelled in a simplified fashion, removing either both the rotors, the empennages and landing gear sponsons. As the reader can appreciate from Figure 4, mesh on the approach surface and internal duct surfaces has been particularly refined in order to properly capture the flow features within the intake#1 flow domain. For the same reason, prismatic volume boundary layer elements thickness and growth rate were set in order to meet the $y+ < 1$ requirement on the duct walls. Refinement regions for the tetra volume mesh on the intake flow domain were defined as well, in order to concentrate the volume elements on the region of interest.

Several turbulence models are available within the CFD tool; for the present analysis Wilcox's two-equation k-ω model with the Menter's Shear-Stress-Transport correction (SST) has been chosen as the most accurate [26], [27].

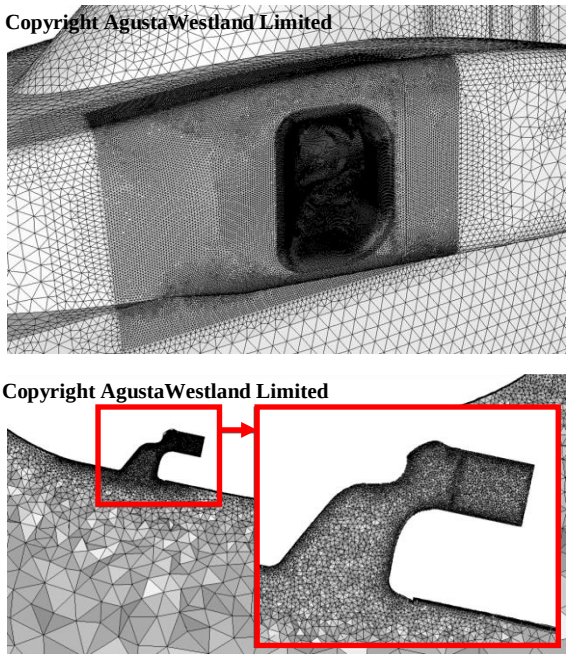

Figure 4: Views of the unstructured surface and volume mesh over the intake#1 flow domain.

The accuracy of the CFD model has been checked by means of comparison against available experimental data, which were obtained during an experimental campaign on a scaled AW101 model at the AgustaWestland Ltd. wind tunnel facility (Figure 5). Simulation results were compared against experimental data in terms of the static pressure distribution over the intake surface,the total pressure loss and total pressure distribution at the AIP, adopting the Rolls Royce DC60 distortion index [2] as a reference parameter.

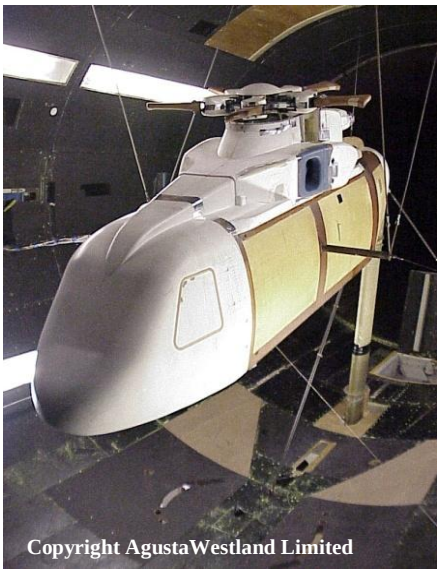

Figure 5: AW101 wind tunnel model; intake performance test at the AW Ltd wind tunnel facility.

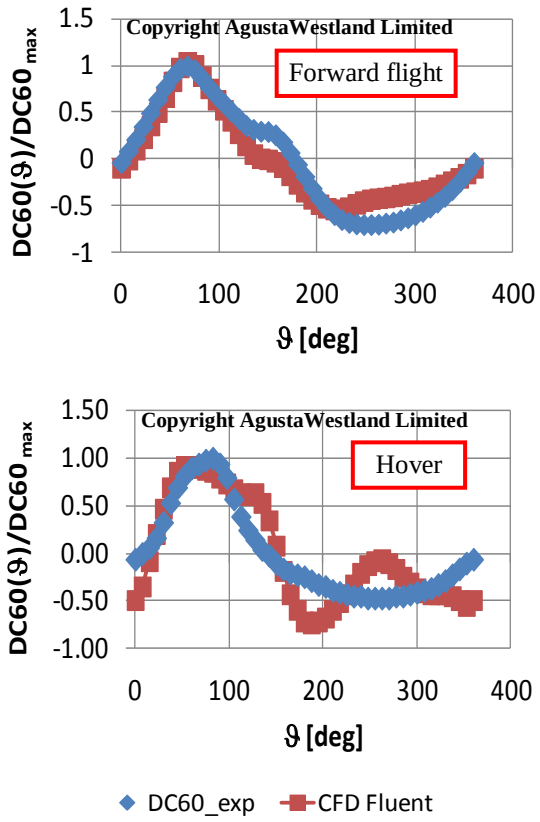

Figure 6: Local DC60 distribution represented along an angular coordinate at the intake#1 AIP; comparison between experimental and numerical results.

Figure 6 shows an example of the comparison between simulation and experiment for the AIP total pressure distortion distribution for two of the cases assessed. Generally the correlation between CFD and experiment was very good, therefore the accuracy of the CFD model was considered to be acceptable for optimisation purposes.

5. SET-UP OF THE PARAMETRIC MODEL

In the first phase, 14 design parameters were identified for the complete geometrical control of the intake#1 duct shape. Those parametric shapes have been generated using the Altair software HyperMesh® by means of the mesh morphing and parameterisation techniques available within the morphing toolbox HyperMorph®. The morphing method selected for the current application is a combination of the *domain/handles* and the *morph volumes* approach [23]: the first allows the application of mesh nodes displacements within a geometrical region (domain) by changing the location of specific, user defined, control points (handles), while the second allows to apply smooth global displacements to nodes placed within a control volume (the morph volume) by morphing the volume itself.

When applied, the nodes displacements can be saved as perturbation vectors and then be reapplied to the baseline model with any given scaling factor. Shape scaling factors become then the design variables for the optimisation problem; the morphed geometry results therefore from the linear combination of the user defined shapes multiplied by their own scaling factors:

$$\boldsymbol{v} = \sum_{i=1}^{14} \alpha_i Sh_i \qquad \textit{Eq. 1}$$

Where:

- $\boldsymbol{v}$ the global displacement vector;
- Sh_i is the i[th] basic shape as visualised in Figure 17to Figure 17;
- α_i is the i[th] shape scaling factor, which is generated by GDEA.

For the present application the α_i factors are defined within the following range:

$$\alpha_i \in [0;1], i = 3,4,5,8,9,11,12,13,14$$
$$\alpha_i \in [-1;1], i = 1,2,6,7,10 \qquad \textit{Eq. 2}$$

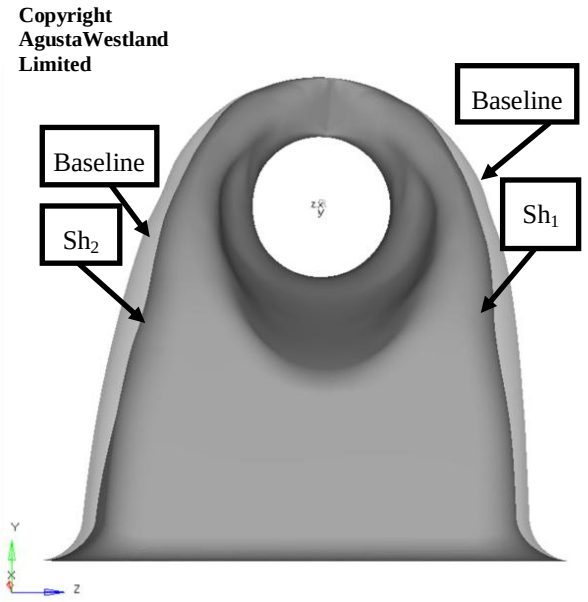

Figure 7: application of Sh_1 parameter with scaling factor α_1=1, and Sh_2 parameter with scaling factor α_2=1.

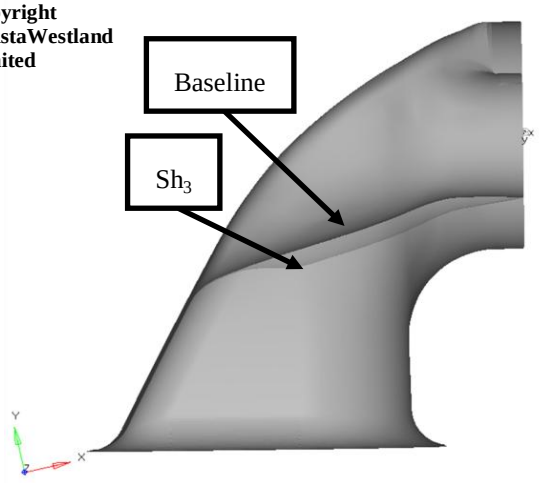

Figure 8: application of Sh_3 parameter; scaling factor applied $\alpha_3=1$.

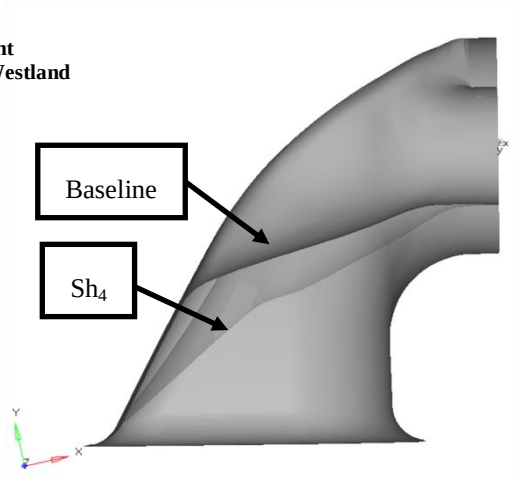

Figure 9: application of Sh_4 parameter; scaling factor applied $\alpha_4=1$.

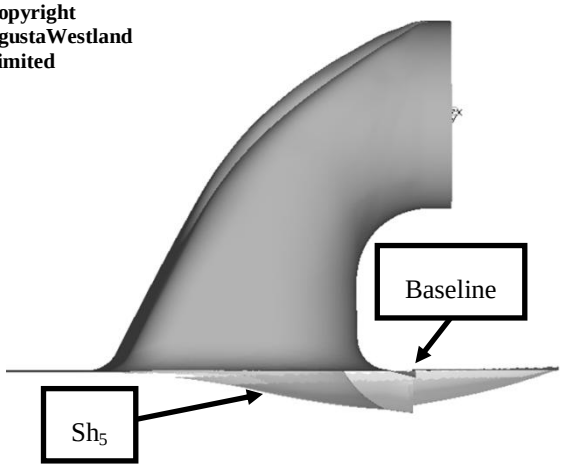

Figure 10: application of Sh_5 parameter; scaling factor applied $\alpha_5=1$.

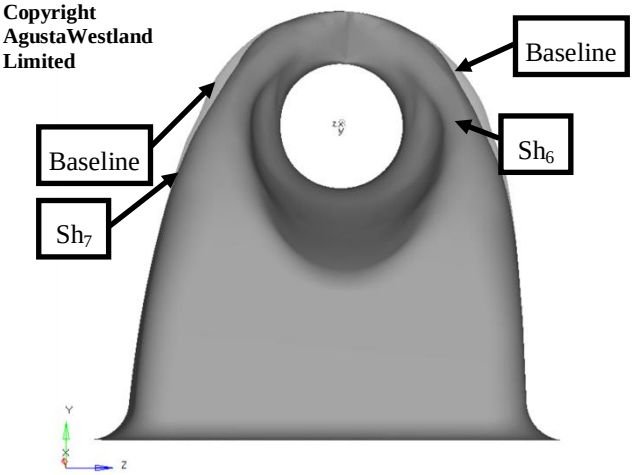

Figure 11: application of Sh_6 parameter with scaling factor $\alpha_6=1$, and Sh_7 parameter with scaling factor $\alpha_7=1$.

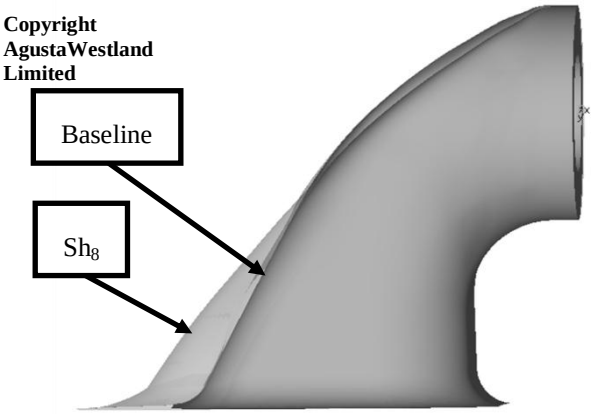

Figure 12: application of Sh_8 parameter; scaling factor applied $\alpha_8=1$.

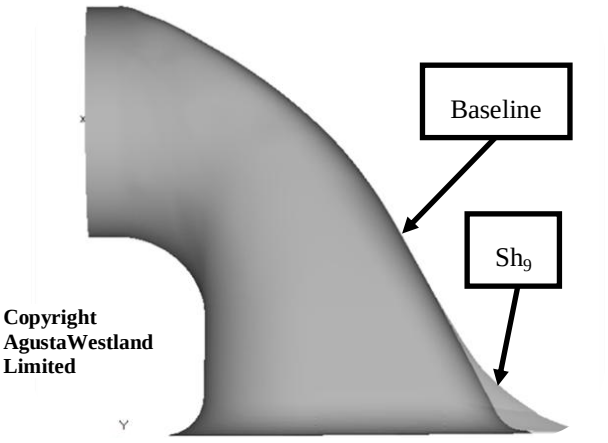

Figure 13: application of Sh_9 parameter; scaling factor applied $\alpha_9=1$.

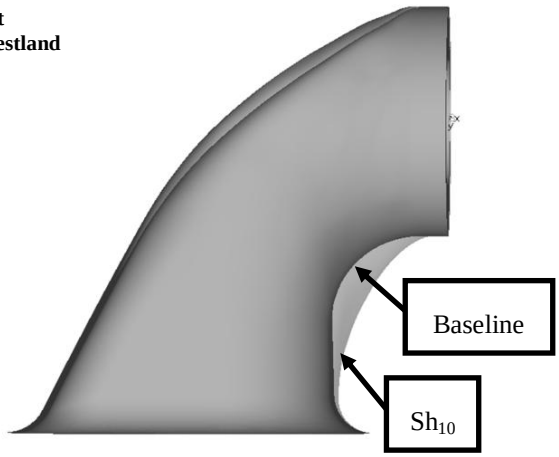

Figure 14: application of Sh_{10} parameter; scaling factor applied $\alpha_{10}=1$.

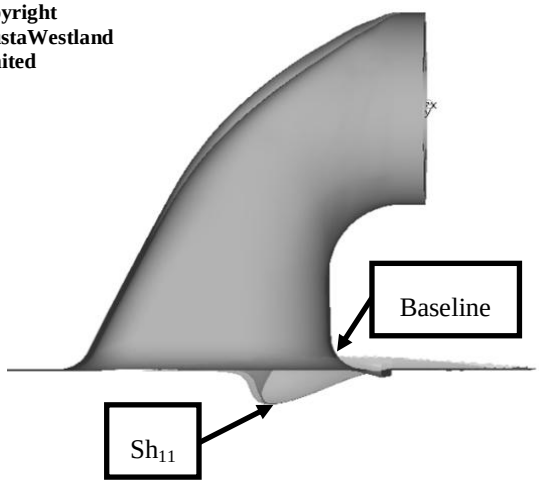

Figure 15: application of Sh_{11} parameter; scaling factor applied $\alpha_{11}=1$.

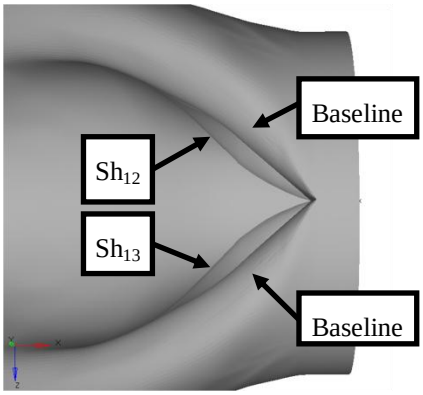

Figure 16: application of Sh_{12} parameter with scaling factor $\alpha_{12}=1$, and Sh_{13} parameter with scaling factor $\alpha_{13}=1$.

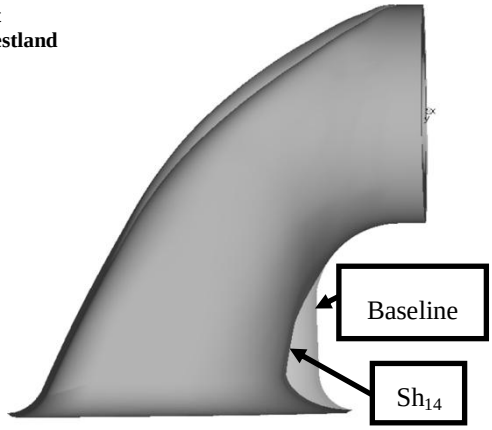

Figure 17: application of Sh_{14} parameter; scaling factor applied $\alpha_{14}=1$.

Basic design shapes have been defined as follows:

- Parameters Sh_1, Sh_2, Sh_6 and Sh_7 control the shape of the two lateral duct walls independently (Figure 7, Figure 11);
- Shapes Sh_3, Sh_4 control the curvature and inclination of the duct front lip (Figure 8, Figure 9);
- Shapes Sh_5, Sh_{11} modify the configuration of rear approach surface, respectively adding a fairing in the normal wall direction and growing a rear lip towards the free stream direction (Figure 10, Figure 15);
- Parameters Sh_8, Sh_9 control the position and curvature of the front wall connection with the approach surface, independently on the two sides. Displacements of the central sections were not allowed because of constraints imposed by the engine bay internal components. For the same reason the two shapes are not symmetrical (Figure 12, Figure 13);
- Shapes Sh_{12}, Sh_{13} modify independently the curvature of the two surfaces connecting into the sharp edge ahead of the AIP (Figure 16);
- Parameters Sh_{10}, Sh_{14} control the rear wall radius (Figure 14, Figure 17).

Maximum displacements have been chosen such as to avoid collisions between the morphed surfaces and the engine bay internal components represented in Figure 3.

6. FORMULATION OF THE OPTIMISATION PROBLEM

With respect to the previous GDEA applications regarding the tilt-rotor ERICA ([20], [21]), the objective function considered for the AW101 intakes optimisation problem is a multi-point function; intake performance have been optimised simultaneously in the two most

relevant helicopter flight conditions, i.e. hover and forward flight cruise, exploiting the multi-objective capabilities of the GDEA code. Following this bi-objective approach, total pressure loss in both hover and forward flight conditions are evaluated by means of two separate CFD simulations and then used by GDEA for assigning the score to the particular design under examination. Total pressure distortion, expressed in the form of the DC60 index [2] are taken into account in the form of a functional constraint: designs resulting in a DC60 value that is higher than the baseline value are *penalised* in their objective function value, with the magnitude of the penalisation driven by the difference in DC60 between the baseline and the actual design. Such multi-objective/multi-point objective function with functional constraints can be mathematically expressed in the following way:

$$Minimise\,\{\boldsymbol{G}(\boldsymbol{x}) = [\boldsymbol{F}(\boldsymbol{x}) + \boldsymbol{PF}(\boldsymbol{x})]\} \qquad Eq.\ 3$$

Where $\boldsymbol{G}(\boldsymbol{x}) = [\boldsymbol{F}(\boldsymbol{x}) + \boldsymbol{PF}(\boldsymbol{x})]$ is the global objective function. $\boldsymbol{F}(\boldsymbol{x})$ is the two component objectives vector containing the total pressure loss (ΔP_T) in hover (first component) and in forward flight (second component) conditions. Mathematically it is formally expressed in Eq. 4.

$$\boldsymbol{F}(\boldsymbol{x}) = \begin{bmatrix} \Delta P_T|\ @\ hover \\ \Delta P_T|\ @\ forward\ flight \end{bmatrix} \qquad Eq.\ 4$$

The penalty function $\boldsymbol{PF}(\boldsymbol{x})$ is expressed in Eq. 5, where the coefficients β and γ control the intensity and shape of the penalty function respectively. For this particular application, γ has been set to 0.5 in order to give the penalty function a convex shape, while β is defined as a fraction of the baseline total pressure loss level in the two flight conditions considered.

$$\boldsymbol{PF}(\boldsymbol{x}) = \begin{bmatrix} 0, if\ DC60 \le DC60_{baseline} \\ \beta\left(\left|\dfrac{DC60 - DC60_{baseline}}{DC60_{baseline}}\right|\right)^{\gamma} \\ if\ DC60 > DC60_{baseline} \end{bmatrix} \qquad Eq.\ 5$$

The design variables vector, **x**, is given by the set of scaling factors in Eq. 6, subject to the variable bounds specified in Eq. 2.

$$\boldsymbol{x} = [\alpha_1, \dots, \alpha_{14}] \qquad Eq.\ 6$$

As explained in the previous section, the design parameters vector affects the baseline geometry by means of the HyperMorph shapes (Sh_i, i=1…14) application, resulting in the morphed configuration mathematically described by Eq. 1.

The number of individuals per generation has been set to 22, while a total number of four generations has been considered for the preliminary optimisation run.

7. SUMMARY OF INTAKE OPTIMISATION RESULTS

The intake#1 optimisation results are discussed within this section; at the time this paper was submitted, four genetic algorithm generations were completed and the associated optimisation results are presented.

Figure 18 shows the preliminary Pareto frontier calculated by the GDEA algorithm: despite the fact that the optimisation process is at a preliminary stage, significant improvements in both hover and forward flight objective functions can be observed. On the left portion of the Pareto frontier, four designs with improved hover performance have been identified, featuring a total pressure loss reduction in the range -13/-30% in hover with significant performance improvement with respect to the baseline design in forward flight cruise as well. Maximum reduction of total pressure loss in forward flight is obtained by the design on the right extreme of the Pareto front: for this particular design the total pressure loss is around 30% lower than the original design. However, hover performance results poorer than the baseline, increasing total pressure loss of 12%. A possible compromise between hover and forward flight intake performance is the solution highlighted in red on Figure 18: hover total pressure loss are reduced by 16% with respect to the original design, while the forward flight total pressure loss experiences a significant 17% reduction. For this design, the distortion level is compliant with the functional constraint in Eq. 5 in forward flight, as a 13% reduction of the DC60 index was observed.

The geometry comparison of the best compromise optimised design with respect to the baseline design, represented in Figure 19 to Figure 24, shows the optimised geometry to be wider than the baseline in the cross sectional direction (negative values for parameters α_1, α_2, α_6, α_7) improving the pressure recovery in the hover condition. The shaping of the rear-lip (parameters α_5, α_{11}) produces an increase of the stagnation pressure on the rear wall region when considering the forward flight condition; this effect increases the energy available for the flow to go around the duct S-bend, improving the intake pressure recovery capabilities.

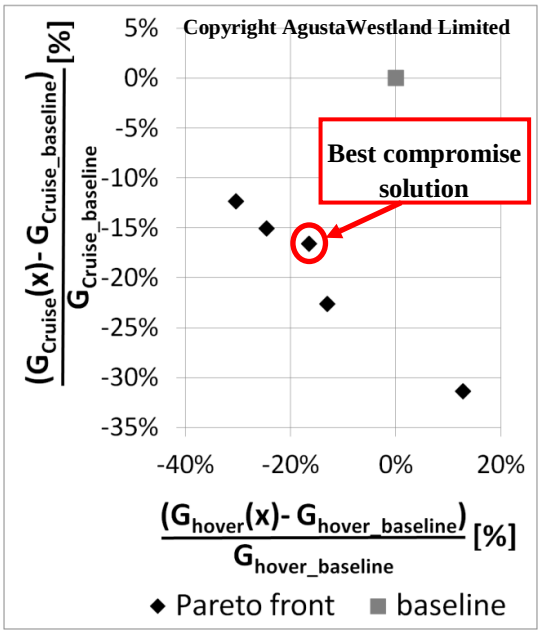

Figure 18: GDEA Pareto frontier, 4th generation; the selected optimal individual is highlighted in red.

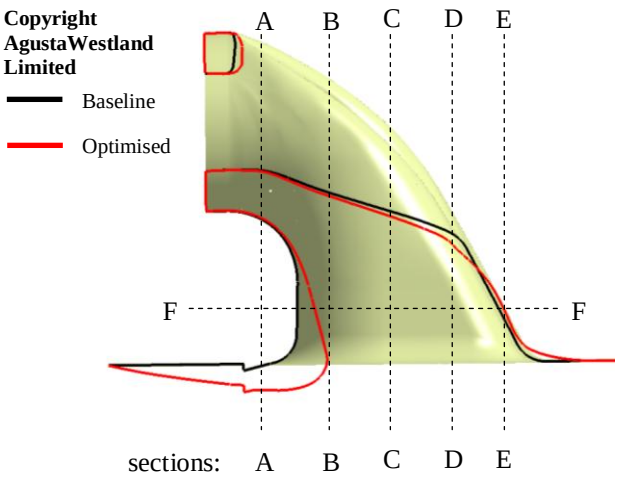

Figure 19: Comparison between baseline and optimised design; intake duct longitudinal section.

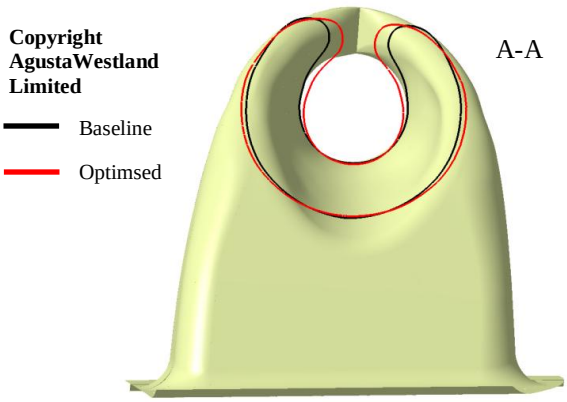

Figure 20: Comparison between baseline and optimised design; intake duct transversal section A-A.

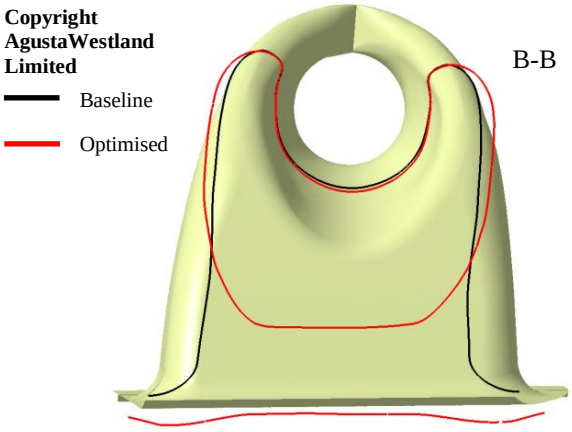

Figure 21: Comparison between baseline and optimised design; intake duct transversal section B-B.

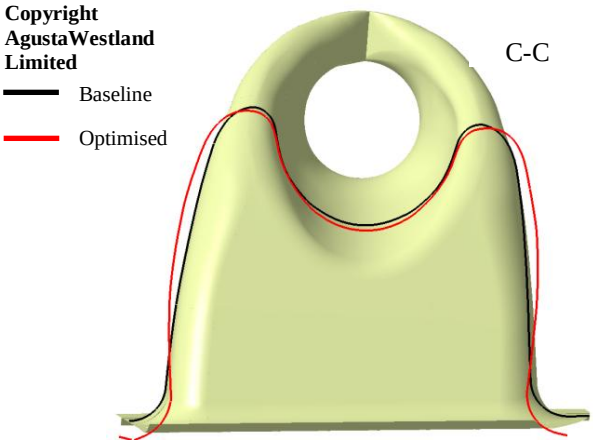

Figure 22: Comparison between baseline and optimised design; intake duct transversal section C-C.

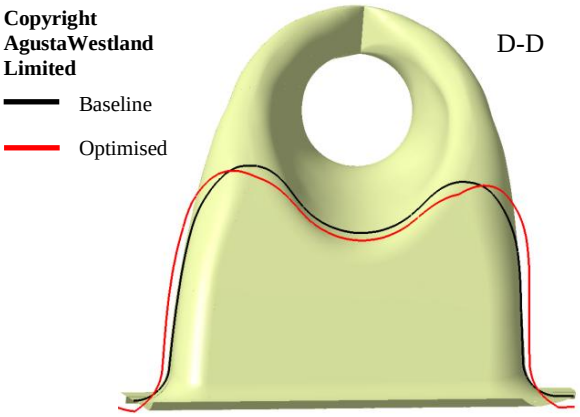

Figure 23: Comparison between baseline and optimised design; intake duct transversal section D-D.

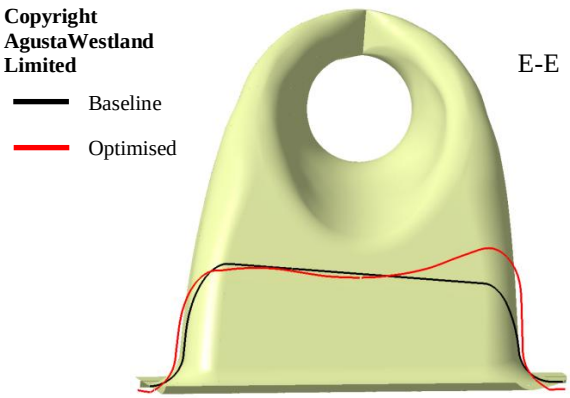

Figure 24: Comparison between baseline and optimised design; intake duct transversal section E-E.

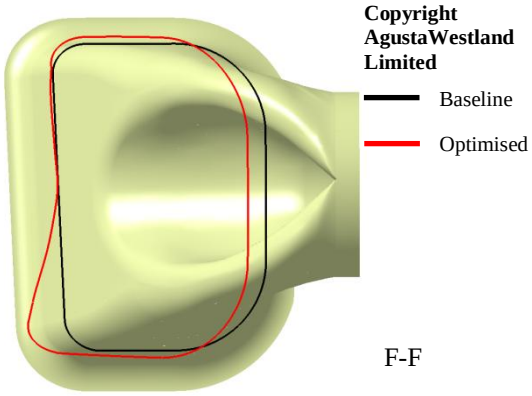

Figure 25: Comparison between baseline and optimised design; intake duct transversal section F-F.

At the same time, the curvature of both the front and rear wall results to be smoother with respect to the original design, reducing the severity of the S-bend (parameters α_8, α_9 for the front wall and α_{14} for the rear wall); these geometry modifications produce, especially in forward flight, more uniform total pressure distribution with a lower level of distortion as depicted on the AIP total pressure contours and efficiency plots on Figure 26 to Figure 29. Comparisons of the local AIP sector average total pressure distribution (Figure 27 and Figure 29) show the more uniform total pressure pattern at the engine face for both hover and forward flight. This result, together with the higher average AIP total pressure value, is expected to improve the engine performance and stability.

8. FUTURE WORK

In parallel with intake#1, optimisation activities on intake#2 are in progress in agreement with the objectives of the HEAVYcOPTer project; the basic geometrical parameterisation and formulation of the optimisation problem for intake#2 has been set up considering strategies very similar to what has been presented for intake#1. However, the different geometry, different flow conditions at the entry section and different system of architectural constraints will make the optimised geometry of intake#2 significantly different from the optimal solution found for intake#1.

A GDEA optimisation will be executed on the AW101 engine exhaust system as well; an existing primary nozzle configuration will be submitted to GDEA based optimisation loop in order to find possible designs to reduce engine back pressure while maintaining the engine bay cooling capabilities of the exhaust system.

1. CONCLUDING REMARKS

The present paper summarises the current progress of the HEAVYcOPTer project, regarding the optimisation of the AW101 engine air intake#1 design. The GDEA based optimisation loop has been applied to the intake duct parametric model and four genetic algorithm generations have been completed at the time this paper was submitted. Despite the very good level of performance characterising the original design (in particular considering hover condition), significant improvement margin has been highlighted for both the flight conditions considered and several designs improving the selected multi-point objective functions have been identified. The discussion reported within the paper demonstrates the strength of the parametric approach chosen: the genetic algorithm GDEA provides an efficient search procedure for alternative designs and optimal solutions while the morphing technology adopted allows solution compatibility with feasibility considerations and industrial constraints.

ACKNOWLEDGMENTS

This research activity is partially funded by the Clean Sky Joint Undertaking related to activities performed within the ITD Green Rotorcraft. The authors would like to thank *Dr. Sebastien Dubois* of the Clean Sky Joint Undertaking for the management monitoring of the HEAVYcOPTer project.

All the research work described throughout this paper was carried out in close cooperation with the AgustaWestland Ltd Aerodynamics department. The authors would like to thank engineers *Nigel Scrase* and *Karl Baverstock* from AgustaWestland for their useful advice and support.

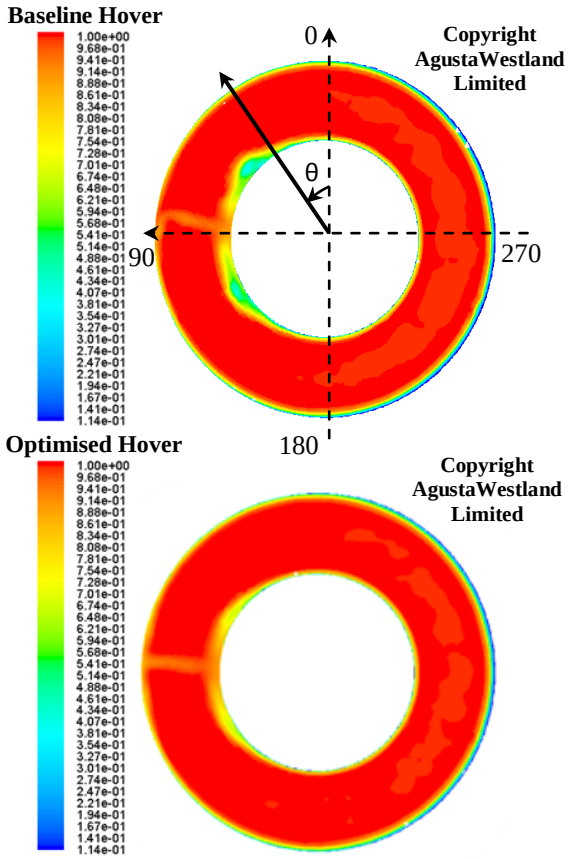

Figure 26: Hover AIP total pressure distribution comparison (normalised by free stream total pressure value); baseline (above) and optimal solution (Below).

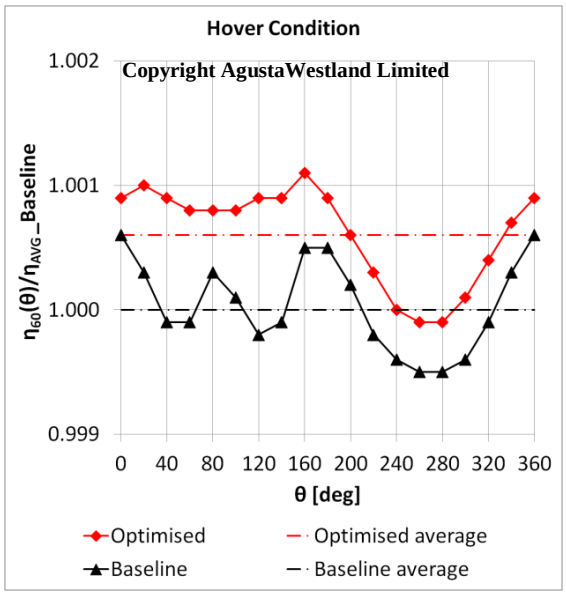

Figure 27: Hover local sector average normalised total pressure distribution for the baseline (black) and optimised (red) designs. Global AIP normalised average efficiency is shown as well. (see Figure 26 for ϑ definition).

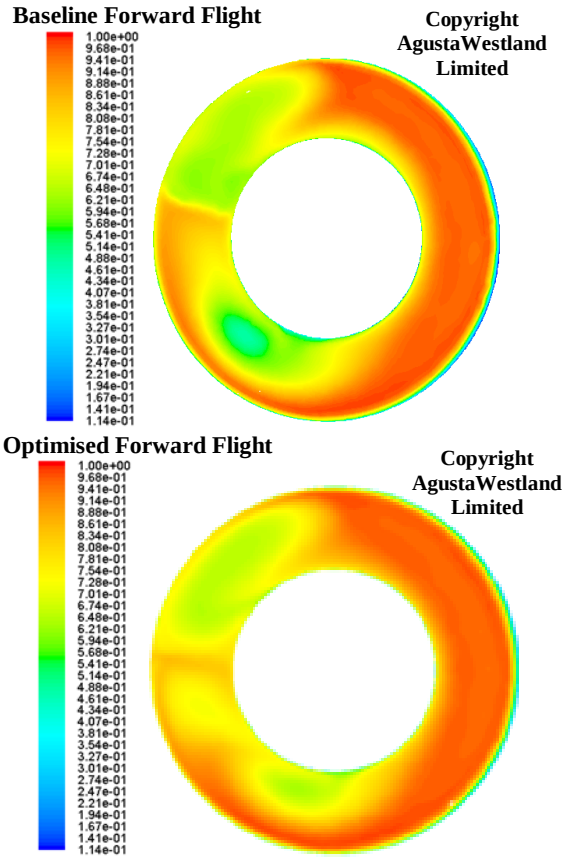

Figure 28: Forward Flight AIP total pressure distribution comparison (normalised by free stream total pressure value); baseline (above) and optimal solution (Below).

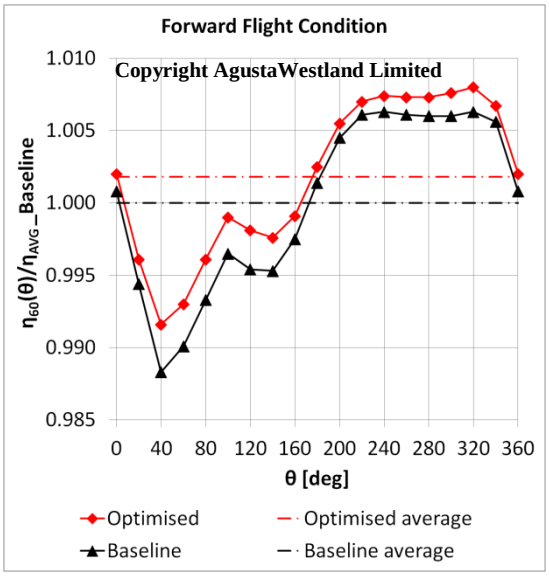

Figure 29: Forward Flight local sector average normalised total pressure distribution for the baseline (black) and optimised (red) designs. Global AIP normalised average efficiency is shown as well. (see Figure 26 for ϑ definition).

REFERENCES

[1] **CleanSky JTI call for proposal** JTI-CS-2010-4-GRC-02-003, *Contribution to optimisation of heavy helicopter engine installation design.*, available on http://www.cleansky.eu/content/homepage/calls, Call SP1-JTI-CS-2010-04, pag. 47.

[2] **Seddon, J. and Goldsmith, L**. *Intake Aerodynamics*. Blackwell Science, 2 edition, 1999.

[3] **Seddon, J**., "*Understanding and countering the swirl in S-ducts: tests on the sensitivity of swirl to fences*," Aeronautical Journal, R.Ae.Soc., 1984.

[4] **Detra, R.W**., "*The secondary Flow in Curved Pipes,*" PhD Thesis, ETH Zurich, 1953.

[5] **Aulehla, F., Schmitz, D.M**., "*Intake swirl and simplified methods for dynamic pressure distortion assessment*," in Intake Aerodynamics, VKI Lecture Series, 1988.

[6] **Farokhi, S**., *Aircraft propulsion*, John Wiley & Sons, Inc. 2009.

[7] **Guo, R. W. and Seddon, J**., "*Some unsteady flow characteristics of two S-shaped intake models tested at high incidence*," University of Bristol, Department of Aeronautical Engineering, Report No. RWG/JS/3/82, 1982.

[8] **Chudý, P., Filakovský, K., Friedl, P.** (2004). *Aerodynamic Analysis of Turboprop Engine Air Intake,* Acta Polytechnica Vol. 44 No. 3.

[9] **Anderson, B.H**., "*Inlets, Ducts and Nozzles*," Proceedings of Aeropropulsion '87, NASA CP-3049, 1987.

[10] **Sinha, R.**, "T*ransient Inlet Nacelle Code*," AIAA Journal of Propulsion and Power, 4, pp. 252-255, 1988.

[11] **Küchemann, D**., **Weber, J**., *Aerodynamics of Propulsion*, New York: McGrawHill, 1953.

[12] **Saha, K., Singh, S.N. and Seshadri, V**. (2007*). Computational Analysis on Flow Through Transition S-Diffusers: Effect of Inlet Shape,* AIAA, Journal of Aircraft, Vol. 44, No.

[13] **Robichaud, M. P., Di Bartolomeo, Heikurinen, W., Habashi, W.G.** (1997). *Turboprop air intake design using 3-D viscous analysis,* AIAA, Aerospace Sciences Meeting & Exhibit, 35th, Reno, NV.

[14] **Zhang, W. L., Knight, D. D., Smith, D**. (2000*). Automated Design of a Three-Dimensional Subsonic Diffuser,* Journal Of Propulsion And Power, Vol. 16, No. 6.

[15] **Benini, E. and Toffolo, A**. *Genetic diversity as an objective in multi-objective evolutionary algorithms*. Evolutionary Computation, MIT press journal, 11(2):151–167, 2003.

[16] Clean Sky website: http://www.cleansky.eu/content/page/reduced-drag-airframe-non-lifting-rotating-parts-grc2.

[17] **Nannoni, F., Giancamilli, G., Cicalè, M**. *Erica: the European advance tilt-rotor*. 27th European Rotorcraft Forum, Moscow, Russia, 11th – 14th September 2001.

[18] **CleanSky JTI call for proposal** JTI-CS-2010-1-GRC-02-004, *Contribution to design optimization of tiltrotor for drag reduction (fuselage/wing junction, nose and landing gear sponsons, empennage)*, available on http://www.cleansky.eu/content/homepage/calls, SP1-JTI-CS-2010-01, pag. 57.

[19] **CleanSky JTI call for proposal** JTI-CS-2009-2-GRC-02-001, *Contribution to the study of the air intake and exhaust integration into a tiltrotor nacelle*, available on http://www.cleansky.eu/content/homepage/calls, SP1-JTI-CS-2009-02, pag. 34.

[20] **Garavello, A., Benini, E., Ponza, R., Scandroglio, A., Saporiti, A.,** *Aerodynamic Optimization of the ERICA Tilt-Rotor Intake and Exhaust System*, Proceeding of the 37th European Rotorcraft Forum, September 13th –15th, 2011, Ticino Park, Italy, Aerodynamic Session, paper ID 191.

[21] **Garavello A., Benini E., Ponza R.**, "*Multi-Objective Aerodynamic Design of Tilt-Rotor Airframe Components by means of Genetic Algorithms and CFD*", Proceeding of the 68th American Helicopter Society Forum, May 1th – 13th, 2012, Fort Worth, Texas (USA), Aerodynamic Session.

[22] **Miste', G., Nibale, T., Garavello, A., Benini, E.** *Assessment of the Engine Installation Performance of a Redesigned Tiltrotor Intake/Exhaust System*, Proceeding of the American Helicopter Society 68th Annual Forum, Fort Worth, Texas, May 1-3, 2012.

[23] Altair HyperMesh 11.0 User Guide.

[24] Ansys Fluent 12.0.16 User Guide.

[25] **Deb, K**. *Multi-Objective Optimisation Using Evolutionary Algorithms*. Wiley, 2001.

[26] **Wilcox, D.C.**. *Turbulence Modeling for CFD*. DCW Industries, Inc., La Canada, California, 1998.

[27] **Menter, F. R.**, "Two-Equation Eddy-Viscosity Turbulence Models for Engineering Applications," AIAA Journal, Vol. 32, No. 8, August 1994, pp. 1598-1605.